Journal of MATERIALS RESEARCH

Article
DOI:10.1557/s43578-021-00345-9

Temperature dependence of the ferromagnetic resonance (FMR) for $Mn_xCo_{1-x}Fe_2O_4$ ($0 \le x \le 1$) nanoparticles

Yeni Sánchez[1], Sarah Briceño[1,2], J. Larionova[3], J. Long[3], Y. Guari[3], Pedro Silva[1,4,a)]

[1] Instituto Venezolano de Investigaciones Científicas (IVIC), Apartado 232, Caracas 1020-A, Venezuela
[2] School of Physical Sciences and Nanotechnology, Yachay Tech University, 100119 Urcuquí, Ecuador
[3] ICGM, Univ Montpellier, CNRS, ENSCM, Montpellier, France
[4] Escuela Politecnica Superior del Litoral (ESPOL), Departamento de Física, FCNM, Campus Gustavo Galindo, Guayaquil, Ecuador
[a)] Address all correspondence to this author. e-mail: pejosi@gmail.com

Received: 1 June 2021; accepted: 9 August 2021; published online: 20 August 2021

Ferromagnetic resonance was used to study the temperature dependence of mixed manganese-cobalt ferrite nanoparticles with a size range between 5 and 42 nm synthesized by the hydrothermal method. Structural characterization was carried out using X-ray diffraction, scanning, and transmission electron microscopy. *M*(H) curves as a function of the Mn^{2+} content at 2.5 and 300 K, and FMR in the temperature range of $80 < T < 700$ K were used for the magnetic characterization. Temperature dependence of the resonance field shows three regions that can be interpreted in terms of agglomeration, dispersion and superparamagnetism in the samples. The H_R and ΔH_{PP} as a function of the temperature and Mn^{2+} content allows us to elucidate the key characteristics of the deviation from the ideal superparamagnetic behavior observed by magnetic measurements and open up new research possibilities for evaluating interparticle interactions in nanoparticles.

Introduction

Spinel ferrite draws its attention to researchers for a long time due to its unique structural and magnetic properties that can be used in transformer cores, magnetic resonance imaging, microwave devices, data storage devices, drug delivery, supercapacitors and biomedical purposes [1, 2]. The suitable magnetic and mechanical properties of ferrites make them worthy for device fabrication. During the development of new technologies, spinel-oxide-type materials are considered competent materials due to their extraordinary physical, chemical, electronic, and magnetic properties [3]. The structural, optical, electrical, and magnetic properties of spinel ferrites also change as the distribution of cations among available A and B sites is modified with doping of impurities, furthermore depending on the physical characteristics, such as particle size, chemical composition, preparation method, surface properties of the particles and interparticle interactions. The magnetic order of especially the surface spins play important role in determining the magnetic properties of a whole ferrite particle due to the high surface-to-volume ratio [4]. Among the various ferrites, cobalt ferrite ($CoFe_2O_4$) nanoparticles have fascinated continuous interest owing to their excellent structural, optical, electrical, magnetic, chemical, catalytic, and thermal properties over the last fifteen years. $CoFe_2O_4$ nanoparticles are gaining increasing interest as gas sensors, photocatalysts, contrast agents for magnetic resonance imaging, targeted drug delivery, cancer imaging and therapy, magnetic hyperthermia, ferrofluids, theragnostic, lithium-ion batteries, magneto-optical devices, and spintronics [5]. It has been found that among the various factors that affect the magnetic, structural, and electrical behavior of nanoferrites particles are their composition, crystal size, and shape. Badoo et al. states that a fine tune of the stoichiometry or composition of the constituents elements is very important to control this properties with the incorporation of Zn, Cd, Zr, and Cu in the ferrite $CoFe_2O_4$ [6–9]. In addition, manganese ferrite has also been of great interest as it has good chemical stability, low coercivity, electrical properties, mechanical hardness, moderate saturation magnetization, and contrast enhancement agents for MRI technology. Recently, the attention of the researchers is focused on the substitution of manganese in cobalt ferrite as

they find distorted structure in the samples. When Mn is added to cobalt ferrite, Mn takes its position in the tetrahedral (A) site, resulting in the movement of Co from the tetrahedral (A) site to the octahedral [B] site, in turn; magnetic properties of the $Co_{1-x}Mn_xFe_2O_4$ system are changed. Currently, interest has been switched towards mixed Mn–Co ferrite nanoparticles with modified structure due to enhanced and emerging properties than that of Mn and Co ferrite individually [10, 11].

Temperature dependence of the Ferromagnetic Resonance Spectra (FMR) provides valuable information on magnetic systems and phase transitions, especially in the assembly of magnetic nanoparticles [12]. For magnetic nanoparticles, a decrease in temperature is accompanied by a shift in the resonance field, an increasingly asymmetric lineshape, and an increased broadening of the resonance lineshape [13]. The FMR of ferrites is important for investigating the magnetic properties at high frequency due to the resonance originates from the interaction between the spin and electromagnetic waves. FMR has been used to study the spin-glass transition in mixed and doped iron oxide nanoparticles. A sudden decrease in resonance field and simultaneous enhancement in spectral linewidth respectively with the decrease in the temperature are accompanied by this characteristics transition [14].

Here, we study the effect of the Mn^{2+} substitution on the structural properties of the $Mn_xCo_{1-x}Fe_2O_4$ ferrite nanoparticles, and the effect of the temperature on the magnetic properties. Moreover, the temperature dependence of the ferromagnetic resonance spectrum for these nanoparticles, with the aim of characterizing the temperature dependence of the spin dynamics of the nanosized system has been focused on. The ferromagnetic resonance spectra were recorded as a function of the Mn^{2+} content ($0 \leq x \leq 1$) in the temperature range $80 < T < 700$ K. Herein, we present a systematic study of the influence of Mn^{2+} content in the resonance field and the peak-peak linewidth. These measurements as a function of temperature have proved to be a powerful tool to distinguish magnetic contributions that otherwise were not clear from direct current (DC) measurements, which have contradictory interpretations in the literature.

Materials and methods

Methods

$Mn_xCo_{1-x}Fe_2O_4$ nanoparticles ($x = 0.00$; 0.25; 0.50; 0.75 and 1.00) have been synthesized using the hydrothermal method. For hydrothermal reactions, all the reagents were of analytical grade and used as received. A mixture of 1 mmol $Fe(NO_3)_3{\cdot}9H_2O$, 0.5 mmol of $Co(NO_3)3{\cdot}6H2O$, and 0.5 mmol of $Mn(NO_3)_3{\cdot}4H_2O$ were dissolved in distilled water in a relation of (2:1:1) respectively, followed by the addition of *4* M KOH solution to adjust the pH at 12. The mixture was then transferred into a Teflon-lined stainless-steel autoclave of 100 mL capacity and stirred until the reactants were completely dissolved. The resulting black precipitates were collected by filtration and washed with deionized water and ethanol, and finally dried in an oven at 60 °C for 24 h. Phase identification, purity, relative crystallinity, structure, and the average size of the samples were determined at room temperature in a polycrystalline sample brand X-ray diffractometer model *Bruker D8* focus using Cu K radiation ($\lambda = 1.5406$ °A) and resolution of 0.002 in 2θ. The structural properties were obtained using a Scanning Electron Microscopy (SEM) model *Philips XL-30* with an analyzer *EDAX* DX-4 for elemental analysis and Transmission Electron Microscopy (TEM) JEOL 1200EXII). The magnetic measurements were carried out in a Quantum Design SQUID magnetometer MPMSXL7 operating between 1.8 and 350 K for DC-applied fields ranging from – 7 to 7 T. Ferromagnetic Resonance measurements were recorded using an EMX BRUKER spectrometer working at the X-band in the temperature range $80 \leq T \leq 700$ K.

Results and discussion

Structural properties

XRD

XRD patterns of $Mn_xCo_{1-x}Fe_2O_4 (0 \leq x \leq 1)$ are shown in Fig. 1a. The samples show the characteristic peaks indexed to the cubic spinel phase of ferrite material with the most intense peak attributed as (311). The *hkl* indexes of the samples are (220), (311), (222), (400), (422), (511), and (440), which indicate the presence of a mixed type cubic spinel structure checked with XRD cards of $CoFe_2O_4$ NPs (*JCPS* file: 22-1086) and $MnFe_2O_4$ PDF-ICDD, 2012). A displacement of the position of (311) peak

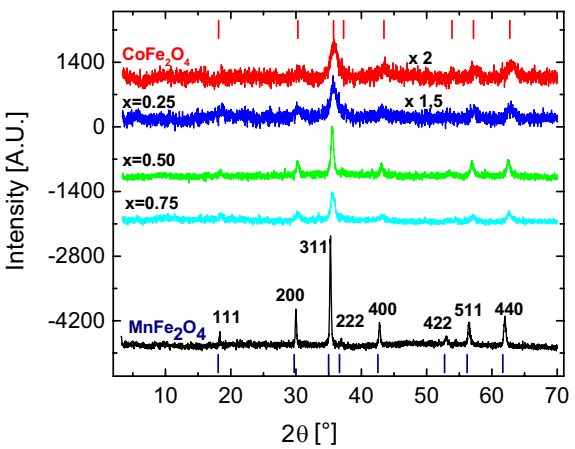

Figure 1: XRD patterns of $Mn_xCo_{1-x}Fe_2O_4 (0 \leq x \leq 1)$ nanoparticles.

with the increase of the concentration of Mn^{2+}, indicates a systematic change of the lattice parameter.

The average particle size, *d,* was calculated using the *Debye–Scherrer* Eq. (1) for the most intense peak (311).

$$d = \frac{\kappa\lambda}{\beta\cos\theta}, \quad (1)$$

where λ is the wavelength of the radiation, θ is the diffraction angle, and β is the FWHM of the diffraction peak. The lattice parameter has been computed using the d-spacing values and the respective (*hkl*) parameters from the classical formula given in Eq. (2)

$$a = \frac{\lambda\left(h^2 + k^2 + l^2\right)}{2\sin\theta}. \quad (2)$$

In Table 1, we show the average size (*d*) and the lattice parameter (*a*), determined using Eqs. (1, 2), as a function of Mn^{2+} content for $Mn_xCo_{1-x}Fe_2O_4$. From the table, an increase with the Mn^{2+} content is observed, except for $x = 0.75$, in which a slight decrease in *d* spacing occurs, maybe due to the rearrangement of the ions in the crystalline structure, that produce a movement of the Mn^{2+} ions from the octahedral to tetrahedral sites [1, 15]. The calculated average sizes of the particles vary in the range of 5–60 nm and the lattice parameter varies in the range of 0.831–0.843 nm, both have a dependence on the Mn^{2+} content, as can be seen in Table 1, obeying the Vegard Law [1, 2]. This increase is attributed to the replacement of Co^{2+} cations having a smaller ionic radius (0.078 nm) by Mn^{2+} cations having a larger one (0.082 nm). When small-sized Co^{2+} ions are substituted with large-sized Mn^{2+} ions, the spinel cobalt ferrite will eventually expand. Doping of Mn^{2+} ions in spinel-type structure will induce uniform strain in the lattice as the material is elastically deformed.

SEM and TEM analysis

SEM and TEM analysis was made over all the samples with the aim of visualizing the structural properties. TEM images for the $Mn_xCo_{1-x}Fe_2O_4$ ($0 \le x \le 1$) nanoparticles are shown in Fig. 2. The mean particle size of the samples was obtained using the TEM measurements and the results are shown in Fig. 2. The average particle size distribution shows that the mean size is relatively close for $x = 0$ and 0.25 and equal to (5 ± 1) and (6 ± 1)nm, respectively (Fig. 2a, b). The shape of these nanoparticles is predominantly spherical. For $x = 0.5$ and 0.75, the size of the nanoparticles increases to 15 ± 1 and 11 ± 1 nm, respectively and the morphology becomes rhomboidal (Fig. 2c, d). For sample $x = 1$, nanoparticles with the mean size 42 ± 1 nm and large nanoparticles also with a rhomboidal shape could be observed in the TEM image in Fig. 2e. The increase of the size of the nanoparticles with the Mn^{2+} substitution is in line with that observed from the XRD analysis. The average size of the nanoparticles and lattice parameter increases with the Mn^{2+} concentrations. Elemental chemical analysis confirms that Co, Mn, Fe, and O ions are present in the nanoparticles and shows that the experimental stoichiometry obtained is similar to the expected one. The SEM micrographs in figure S.1 (Supplementary Information), show the formation of large grains without a defined shape.

Magnetic properties

Magnetization curves

Figure 3a–e show the magnetization curves at 300 K and Fig. 3f–j exhibit the magnetization curves at 2.5 K of $Mn_xCo_{1-x}Fe_2O_4$ at different Mn^{2+} content. The magnetization values at 3 kOe, M_S, remanent magnetization, M_r, and the coercive field, H_c, are summarized in Table 1. M_S ranges between 50 and 75 emu/g for all the samples at 300 K.

These M_S values are lower than the ones of corresponding bulk materials (110 emu/g for $MnFe_2O_4$ and 93.9 emu/g for $CoFe_2O_4$) [16] probably due to the effects of surface spin disorder or the spins canting [17, 18]. The Magnetization curves, measured at 2.5 K, showed hysteresis loops corresponding to a ferromagnetic state of the samples, and for the measurements, at room temperature, we observe no hysteresis loop in agreement

TABLE 1: Structural and magnetic properties of $Mn_xCo_{1-x}Fe_2O_4$ ($0 \le x \le 1$) system.

				300 K				2.5 K			
(*x*)	[d]XRD, (nm)	[d]TEM, (nm) ± 1	*a*, (nm) ±0.001	H_c, (Oe) ±5	M_s, (emu.g^{-1}) ±1	M_r, (emu.g^{-1}) ±1	K_1, [×10^{6}erg/cm^3] ±0.01	H_c, (Oe) ±40	M_s, (emu.g^{-1}) ±2	M_r, (emu.g^{-1}) ±1	K_1, (×10^{6}erg/cm^3) ±0.01
0.00	6 ± 1	5	0.831	25	55	1	0.24	11,180	65	40	0.36
0.25	9 ± 1	6	0.834	20	60	1	0.38	11,660	70	50	0.32
0.50	19 ± 2	15	0.838	330	65	15	0.10	8520	85	65	0.59
0.75	12 ± 2	11	0.840	45	50	3	0.08	7060	70	50	0.37
1.00	32 ± 3	42	0.843	40	75	5	0.06	110	100	15	0.08

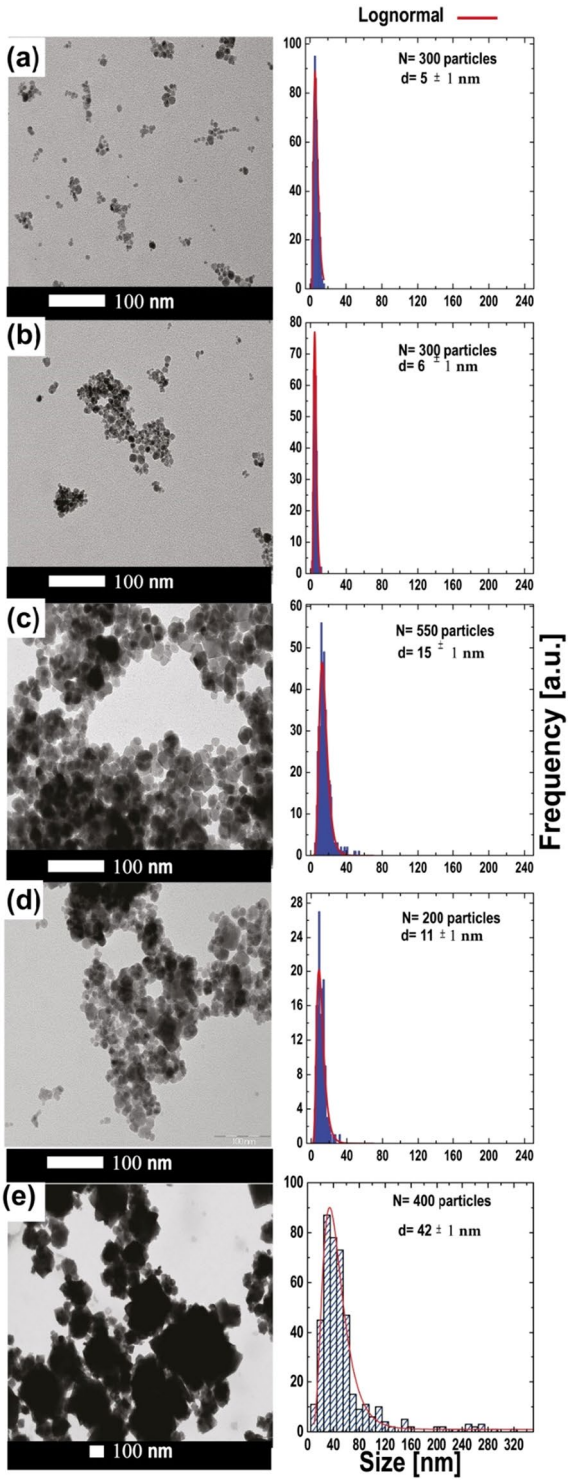

Figure 2: Transmission Electron microscopy (TEM) images for $Mn_xCo_{1-x}Fe_2O_4$ ($0 \le x \le 1$) system, (a) $CoFe_2O_4$ (b) $Mn_{0.25}Co_{0.75}Fe_2O$ (c) $Mn_{0.50}Co_{0.50}Fe_2O_4$ (d) $Mn_{0.75}Co_{0.25}Fe_2O_4$ and (e) $MnFe_2O_4$.

with a superparamagnetic state. At low temperatures, the magnetization curves have two important characteristics, an open hysteresis loop and unsaturation at 3 kOe for all samples except $x = 1$. The dependence of the coercive field, H_c, as a function of the Mn^{2+} content (Fig. 4a) shows a maximum in the coercive field for $x = 0.5$ at 300 K, while it is not present at 2.5 K. It is important to note that the average size of the nanoparticles also has a local maximum at this Mn^{2+} concentration [4]. At 2.5 K a monotonic decrease in H_c with the Mn^{2+} content may be observed [19]. Figure 4b displays the dependence of the M_S as a function of the Mn^{2+} content at 2.5 and 300 K. A linear increase of the M_S as a function of the Mn^{2+} content is observed at 300 and 2.5 K. The magnetization increases in all the range studied, except for $x = 0.75$ at room temperature, due to the substitution of Mn^{2+} (5.92 μ_B) ions and Co^{2+} (3.87 μ_B) in the octahedral sites [20, 21]. At 2.5 K the saturation of the magnetization is not observed even at a relatively high applied field of 3 kOe, Topkaya et al. suggest the existence of surface spins disorder due to symmetry broken for antiferromagnetic interactions [4]. Due to a strong coupling or pinning between disordered surface spins and ordered core ones, the former are not easily aligned even with a high applied field [4]. Figure 4c shows the remanent magnetization M_r as a function of the Mn^{2+} content at 300 K and 2.5 K. Small M_r values are observed for all concentrations studied at 300 K similarly to the behavior obtained for the coercive field, these results are in accordance with a superparamagnetic ordering in the nanoparticles at this temperature. When the temperature is lowered to 2.5 K, a slightly linear increase in the remanent magnetization up to $x = 0.75$, due to changes in the Mn^{2+} distribution, is observed. At 2.5 K, M_r exhibits an out-of-trend behavior with an increment for sample $x = 0.5$, besides that, an abrupt decrease for $MnFe_2O_4$. Similarly, the remanent magnetization at 300 K shows a linear behavior, except for $x = 0.5$, where a marked increase is observed may be due to the particle size distribution. The corresponding sizes for $x = 0.0$, 0.25, and 0.75 are in accordance with particles in the superparamagnetic state, but $x = 0.5$ are in a monodomain state where the remanence magnetization is greater than for the former [22, 23]. The uniaxial anisotropy constant was determined using the LAS law, Eq. (3) [24].

$$M = M_s\left[1 - \frac{8}{105}\left(\frac{K_1}{M_s H}\right)^2\right] + \kappa H. \qquad (3)$$

where the numerical coefficient 8/105 holds for random polycrystalline specimens with cubic anisotropy and *K1* is the uniaxial anisotropy constant. The term κH is included to take into consideration of the observed increase in the spontaneous magnetization at high fields, known as the forced magnetization, with the parameter K being the high-field susceptibility. In general, the forced magnetization term is necessary to fit the hysteresis curves at higher temperatures and higher fields [24]. The uniaxial anisotropy constant of $Mn_xCo_{1-x}Fe_2O_4$ system as a function of the Mn^{2+} content at 300 K and 2.5 K, are plotted in Fig. 4d. The calculated uniaxial anisotropy constant is ranging

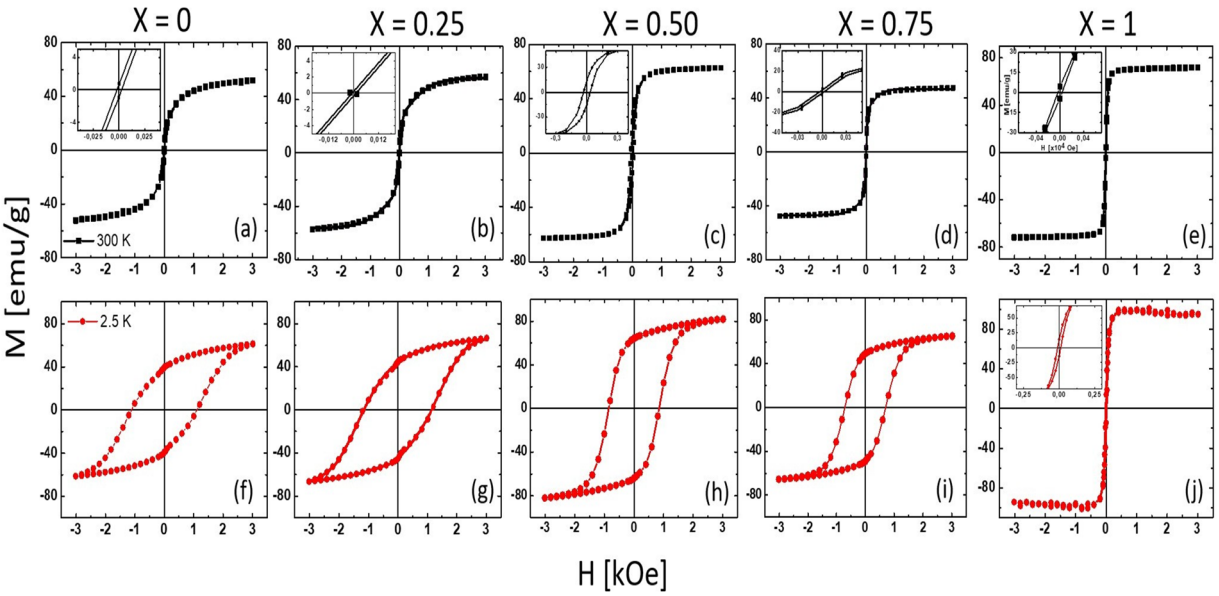

Figure 3: Magnetization versus applied magnetic field of $Mn_{1-x}Co_xFe_2O_4$ ($0 \le x \le 1$) nanoparticles, at (a–e) 300 K (f–j) 2.5 K.

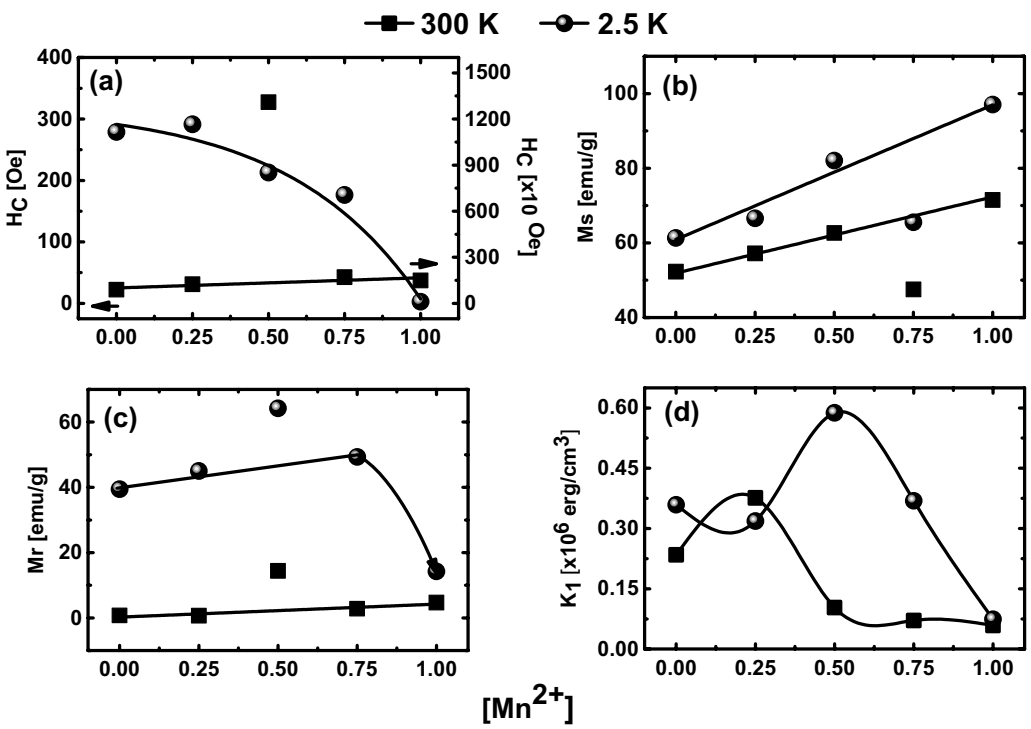

Figure 4: Dependence of the coercive field (*Hc*), (b) maximum magnetization (*Ms*), (c) remanent magnetization (*Mr*), and (d) anisotropy constant (K_1) of $Mn_xCo_{1-x}Fe_2O_4$ ($0 \le x \le 1$), as a function of the Mn^{2+}content, at 300 K and 2.5 K.

from 0.06 to 0.38×10^6 erg/cm^3 at 300 K, and 0.08 to 0.59×10^6 erg/cm^3 at 2.5 K. In both cases, low and room temperatures, the uniaxial anisotropy constant is nearly the same for $x = 1$ sample ($MnFe_2O_4$). K_1 takes its maximum value at room temperature when $x = 0.25$, at 2.5 K this maximum shift to $x = 0.5$. It may be due to the largest contribution of Co^{2+} ions, located at the octahedral sites *B* of the spinel structure [4], while for the $x > 0.5$, the cobalt ions have a smaller contribution to this parameter due to the reduction of the occupation of Co^{2+} ions on the sites B with a decrease in the anisotropic properties of the Co^{2+} ions [25].

Ferromagnetic resonance (FMR)

The temperature dependence of the ferromagnetic spectra, in the temperature range $90 < T < 670$ K as a function of the Mn^{2+} content, was investigated to evaluate the effect of the temperature and the concentration of Mn^{2+} on the dynamic properties of the samples. The FMR condition for magnetic materials is given by:

$$\omega = \gamma H_{\text{eff}} \tag{4}$$

where ω, γ, and H_{eff} are the angular frequency, the gyromagnetic ratio, and the effective magnetic field, respectively. If the resonance field value (3400 Oe, in $g = 2$) is different from the one observed, this indicates that there is an interaction between magnetic nanoparticles [4]. Therefore, the effective magnetic field can be described by the sum of two terms:

$$H_{\text{eff}} = H_R + H_{\text{int}}, \tag{5}$$

where the first term of the right side of Eq. (5) represents the applied external magnetic field, this is the resonance field H_R, the second term represents the internal magnetic field, defined as follows:

$$H_{\text{int}} = H_{\text{dem}} + H_{\text{dip}} + H'_{\text{dip}}, \tag{6}$$

where H_{dem} is the internal field, due to demagnetization, H_{dip} is the internal field, due to the dipole–dipole interaction between neighboring magnetic nanoparticles, and H'_{dip} is the internal field that arises from the dipole–dipole interaction between agglomerates.

Figure 5 shows the FMR spectra at room temperature for all the Mn^{2+} concentrations studied. For the $CoFe_2O_4$ nanoparticles, a single very broad signal with zero field absorption centered around 150 mT is observed. The doping with Mn^{2+} gradually produces a narrowing in the FMR spectra up to reach the $x = 1$ concentration ($MnFe_2O_4$) in which a very clear and intense spectrum with two signals, one of them the high field signal around 340 mT, and the low field signal around 250 mT.

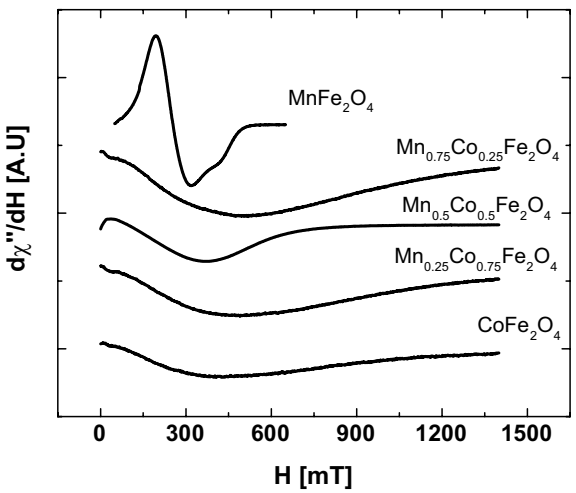

Figure 5: FMR spectra of the $Mn_xCo_{1-x}Fe_2O_4$ ($x = 0.0, 0.25, 0.5, 0.75, 1.0$) ferrite at 300 K.

Figure 6 shows the temperature dependence of the FMR spectra for samples at $x = 0.75$ (Fig. 6a) and $x = 1$ (Fig. 6b) in the temperature range $100 < T < 600$ K. Figure 6c and d, exhibit the temperature dependence of the resonance field (H_R) and peak-to-peak linewidth (ΔH_{PP}) for two samples, $x = 0.75$ and $MnFe_2O_4$ ones. Three regions can be observed in all samples containing Co^{2+} ions, but not for $MnFe_2O_4$. Their analysis shows different behaviors according to temperature. In region III (high field region) a near-constant resonance field is observed, which is in accordance with a superparamagnetic state of the samples where above the blocking temperature the resonance field is temperature independent. In this region, a slow increase of ΔH_{PP} with temperature decrease, agrees with an increase of dipolar interactions, due to the decrease in thermal energy. In region II (intermediate field region), a decrease in H_R and an increase in ΔH_{pp} with the decrease of temperature is observed. This behavior is in accordance with both, the blocking of the magnetic moments of the nanoparticles and with the appearance of dipolar interparticle interactions. This latter increases the dipolar field in Eq. (5) and consequently decreases H_R (Eq. 4) up to a minimum value, when nanoparticles begin to agglomerate. Resonance field behavior in the III–II regions can be explained using the *Landau-Lifshitz* dynamics [26] and as suggested by Kodama [27], as the temperature decreases, the surface spins freeze in the direction of the magnetic DC field. The Resonance field behavior at low field can be explained by the surface spin disorder. An exchange coupling between the spins on the surface and spins of the nucleus, which causes unidirectional anisotropy with an easy axis along the direction of the field [28], bringing therefore a decrease in the resonance field [29]. In region I (low field region) an increase in H_R and ΔH_{PP} with the decreasing of the temperature up to $T \sim 180$K is observed. The resonance field reaches a minimum value and then increases, which may occur because of the formation of nanoparticles agglomerates. This latter induces an appearance of dipolar interactions between agglomerates in addition to the interparticle dipolar interactions. The former is more weakly than the latter, so the resonance field begins to increase. According to the *Landau-Lifshitz* model [30] in the temperature range $180 \leq T \leq 360K$, ΔH_{PP} scales as l/T as predicted by the model, which states this behavior for aggregates of particles. Below $T \sim 180$K, the resonance field and the peak-to-peak linewidth becomes almost constant showing a paramagnetic like behavior. In the three regions, the linewidth increases continuously, while the temperature decreases. However, a slight change in the slope of the linewidth at the blocking temperature for the NPs and just before the nanoparticles begin to agglomerate. In

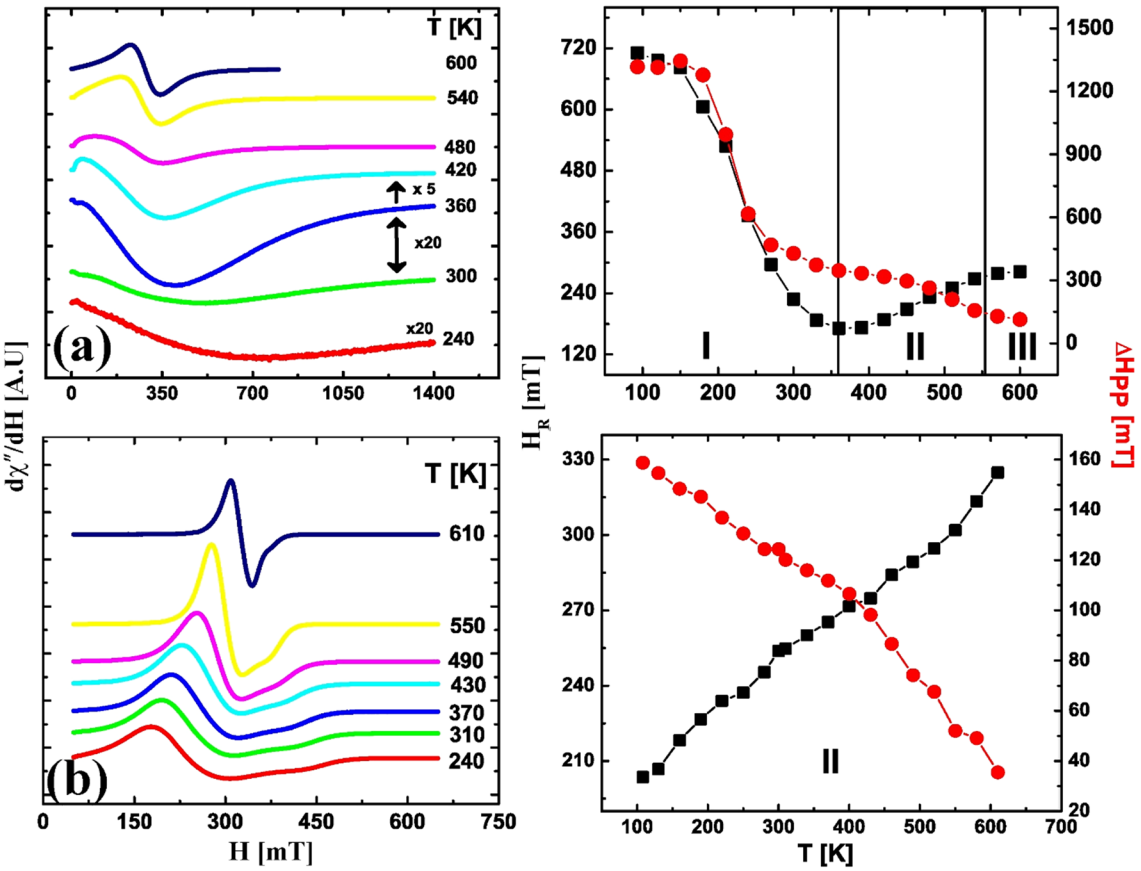

Figure 6: Evolution of the signal of resonance of $Mn_xCo_{1-x}Fe_2O_4$ and dependence of H_R and ΔH_{PP} as a function of the temperature at (a) $x = 0.75$ and (b) $x = 1$.

the $MnFe_2O_4$ sample, two signals very close each to other in almost the entire temperature range studied are observed, the high field signal may be associated with a paramagnetic phase of manganese in very low proportion; instead for ferrites containing cobalt, they show a unique and symmetric signal above of 400 K that can be associated to superparamagnetic behavior of the system [31]. $MnFe_2O_4$ shows a different behavior than that shown by mixed Mn–Co ferrites. For this sample, the resonance field shows a monotonous growth with the increase in temperature, this behavior is typical of ferrimagnetic systems where the increase in thermal energy gradually decreases the local fields. On the other hand, the linewidth shows a change in slope around $T = 430$ K. Even when the superparamagnetic blocking temperature is not reached, this slope change must be related to the start of the superparamagnetic behavior of the nanoparticles. It is important to emphasize that the behavior of the resonance field and the linewidth in $MnFe_2O_4$ is different from that of mixed ferrites because the size of the former is large enough to be multidomain particles, while the latter is essentially monodomain particles.

Figure 7 shows the dependence of H_R and ΔH_{PP} as a function of Mn^{2+} content for $Mn_xCo_{1-x}Fe_2O_4$ at 300 K. A decrease

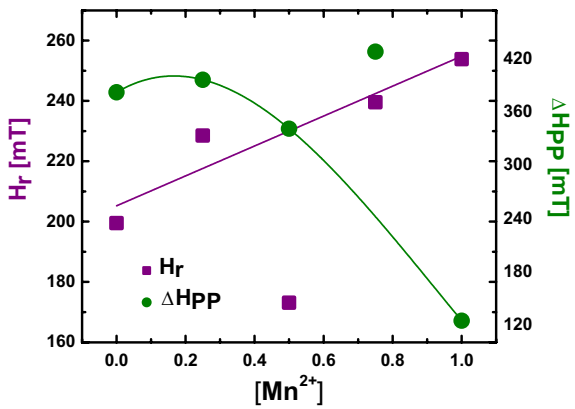

Figure 7: H_R and ΔH_{PP} as a function of the manganese content at 300 K.

in ΔH_{PP} with the increase in the Mn^{2+} content is observed, except for sample $x = 0.75$, which is out of the tendency, in accordance with the results for magnetization and the particle size obtained with XRD. A small saturation magnetization in conjunction with a small particle size presents a favorable situation for interparticle magnetostatic interaction, which results

in a broadening of ΔH_{PP} [32]. An abrupt decrease in linewidth is observed for the $MnFe_2O_4$ sample, indicating a decrease in dipole interactions of the nanoparticles. The behavior of ΔH_{PP} as a function of the Mn^{2+} content agrees with those reported by Arda et al. [33] for the $Zn_{1-x}Co_xO$ system synthesized by the sol–gel method. The resonance field H_R linearly increases due to the occupation of Mn^{2+} at octahedral sites. The presence of Mn^{2+} at the octahedral sites causes a decrease in the magnetic moment of sublattice B, which results in a decrease in the total magnetic moment, this in accordance with a decrease in the internal fields, and therefore an increase in H_R is observed. An anomalous decrease in the H_R behavior for $x = 0.5$ is observed in agreement with the behavior of the remanent magnetization.

The spin–spin relaxation time constant (τ) as a function of temperature for all samples is shown in Fig. 8. The spin–spin relaxation time constant is calculated with the help of the following equation:

$$\tau = \frac{\hbar}{g\beta\sqrt{3}\Delta H_{PP}}, \tag{7}$$

where h is the Planck's constant (6.626×10^{-34} J s), $\hbar = h/2\pi$, and β is a Bohr magneton (9.27×10^{-24} J T^{-1}). All mixed Mn^{2+}-Co^{2+} samples, except the sample $x = 0.50$, present similar behavior: at low temperatures ($T < 400$K), a quasi-constant behavior of the spin–spin relaxation time with a maximum reached at 225 K for $x = 0$, and 255 K for $x = 0.25$ and 0.75, respectively. This maximum may be correlated with the temperature at which the dipolar interaction between agglomerates of the nanoparticles begins to dominate over the dipolar interaction between nanoparticles. Above $T = 400$K, an abrupt increase in the spin–spin relaxation time is observed. This behavior is correlated with a decrease in the ΔH_{PP} in accordance with the decrease in the dipole–dipole interactions. The temperature dependence of the spin–spin relaxation time for $x = 0.50$ is shown in Fig. 8a. The maximum on this curve at $T = 230$ K can be correlated with the formation of agglomerates. Then, a continuous decrease in the relaxation time is observed. It can be seen that the spin–spin relaxation time is one order of magnitude higher than those for the other samples in agreement with the results obtained for the magnetization curves. Note that a continuous increase in the spin–spin relaxation time in all temperature range can be observed for $MnFe_2O_4$ (Fig. 8c), with a change in the slope at near $T = 400$K, as for the rest of the samples, except for $x = 0.5$.

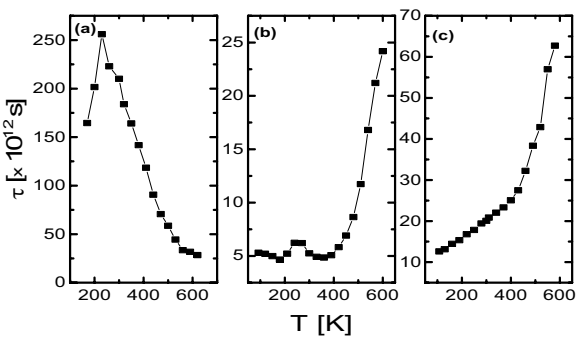

Figure 8: Temperature dependence of the relaxation times, τ, for $Mn_xCo_{1-x}Fe_2O_4$ (a) $x = 0.5$, (b) $x = 0.75$ and (c) $x = 1.0$ nanoparticles.

Summary

A series of spherical and rhomboidal ferrites nanoparticles of $Mn_xCo_{1-x}Fe_2O_4$ with an average size range 5–42 nm was obtained using the hydrothermal method. Their magnetic properties show a ferromagnetic behavior at low temperatures and a superparamagnetic behavior at room temperature. The temperature dependence of the ferromagnetic resonance (FMR) spectra shows three regions. The resonance field increases when the temperature decreases in region *I* and the peak to peak linewidth follows a Landau-Lifshitz behavior (product of the agglomeration of the nanoparticles). In region *II*, the resonance field increases with temperature, following the *Landau-Lifshitz* model. The linewidth in this region decreases with temperature with a slow change in the slope in agreement with weakening in dipole–dipole interactions. Finally, region *III* shows a superparamagnetic behavior throughout the range of temperature as a consequence of modification in the magnetic regime (vanishing of the magnetic moments blocking). Here, a decrease in the linewidth with temperature in agreement with a superparamagnetic behavior is observed. The peak-to-peak linewidth shows a slight decrease with the Mn^{2+} content. This suggests that dipolar interactions become weaker, while the resonance field increases with the concentration of Mn^{2+}. However, sample $x = 0.5$ presents an exception from this behavior because Mn^{2+} occupy the octahedral sites, which provides a decrease in the magnetic moment of sublattice *B*. This situation induces a decrease in the total magnetic moment. Spin–Spin relaxation time indicates the temperature at which the nanoparticles begin to agglomerate and the temperature at which the systems have shown a superparamagnetic behavior.

Acknowledgments

Thanks to the FONACIT for the financing of the PEII 2011001368 and MPPCTI- ECOS-Nord (V13PS01). The authors thank the CNRS, the University of Montpellier, and the Venezuelan Institute for Scientific Research (*IVIC*) for financial support. We also thank the Platform of Analysis and Characterizations of ICGM for measurements.

Declarations

Conflict of interest On behalf of all authors, the corresponding author states that there is no conflict of interest.

Supplementary Information

The online version contains supplementary material available at https://doi.org/10.1557/s43578-021-00345-9.

References

1. S. Nasrin, F.U.Z. Chowdhury, S.M. Hoque, Study of hyperthermia temperature of manganese-substituted cobalt nano ferrites prepared by chemical co-precipitation method for biomedical application. J. Magn. Magn. Mater. **479**, 126–134 (2019). https://doi.org/10.1016/j.jmmm.2019.02.010
2. L.S. Ghadimi, N. Arsalani, I. Ahadzadeh, A. Hajalilou, E. Abouzari-Lotf, Effect of synthesis route on the electrochemical performance of CoMnFeO nanoparticles as a novel supercapacitor electrode material. Appl. Surf. Sci. **494**, 440–451 (2019). https://doi.org/10.1016/j.apsusc.2019.07.183
3. S.M. Ansari, K.C. Ghosh, R.S. Devan, D. Sen, P.U. Sastry, Y.D. Kolekar, C.V. Ramana, Eco-friendly synthesis, crystal chemistry, and magnetic properties of manganese-substituted $CoFe_2O_4$ nanoparticles. ACS Omega **5**(31), 19315–19330 (2020). https://doi.org/10.1021/acsomega.9b02492
4. R. Topkaya, Ö. Akman, S. Kazan, B. Aktas, Z. Durmus, A. Baykal, Surface spin disorder and spin-glass-like behaviour in manganese-substituted cobalt ferrite nanoparticles. J. Nanopart. Res. **14**, 1156 (2012)
5. P. Monisha, P. Priyadharshini, S.S. Gomathi, K. Pushpanathan, Influence of Mn dopant on the crystallite size, optical and magnetic behavior of $CoFe_2O_4$ magnetic nanoparticles. J. Phys. Chem. Solids **148**, 109654 (2021)
6. S. Asiri, M. Sertkol, S. Guner, H. Gungunes, K.M. Batoo, T.A. Saleh, H. Sozeri, M.A. Almessiere, A. Manikandan, A. Baykal, Hydrothermal synthesis of CoyZnyMn1−2yFe2O4 nanoferrites: magneto-optical investigation. Ceram. Int. **18**(5), 5751–5759 (2018). https://doi.org/10.1016/j.ceramint.2017.12.233
7. S.S. Desai, S.E. Shirsath, K.M. Batoo, S.F. Adil, M. Khan, S.M. Patange, Influence of Zn-Zr substitution on the crystal chemistry and magnetic properties of $CoFe_2O_4$ nanoparticles synthesized by sol-gel method. Phys. B **596**, 412400 (2020). https://doi.org/10.1016/j.physb.2020.412400
8. K.M. Batoo, E.H. Raslan, Y. Yang, S.F. Adil, M. Khan, A. Imran, Y. Al-Douri, Structural, dielectric and low temperature magnetic response of Zn doped cobalt ferrite nanoparticles. AIP Adv. **9**, 055202 (2019). https://doi.org/10.1063/1.5078411
9. N. Boda, K.C. Naidu, K.M. Batoo, G.H. Joice, J.L. Naik, D. Ravinder, Structural, morphological and electronic properties of cadmium cobalt ferrite nanoparticles. Biointerface Res. Appl. Chem. **10**(1), 4752–4763 (2020). https://doi.org/10.33263/BRIAC101.752763
10. A. Jamil, M.F. Afsar, F. Sher, M.A. Rafiq, Temperature and composition-dependent density of states extracted using overlapping large polaron tunneling model in MnxCo1 xFe2O4 (x = 0.25, 0.5, 0.75) nanoparticles. Phys. B **509**, 76–83 (2017)
11. M.M. Hossen, S. Nasrin, M.B. Hossen, Structural, dielectric and magnetic properties of Mn2+ doped cobalt ferrite nanoparticles. J. Magn. Magn. Mater **599**, 165726 (2019)
12. R. Rai, K. Verma, S. Sharma, S.S. Nair, M.A. Valente, A.L. Kholkin, N.A. Sobolev, Study of structural and ferromagnetic properties of pure and Cd doped copper ferrite. J. Phys. Chem. Solids **72**(7), 862–868 (2011). https://doi.org/10.1016/j.jpcs.2011.04.002
13. H. Bayrakdar, O. Yalçın, U. Cengiz, S. Özüm, E. Anigi, O. Topel, Comparison effects and electron spin resonance studies of α-Fe_2O_4 spinel-type ferrite nanoparticles. Spectrochim. Acta A **374**, 696–702 (2014)
14. M.R. Diehl, J.Y. Yu, J.R. Heath, G.A. Held, H. Doyle, S. Sun, C. Murray, Crystalline, shape and surface anisotropy in two morphologies of superparamagnetic cobalt nanoparticles by ferromagnetic resonance. J. Phys. Chem. **33**, 7913–7919 (2001)
15. A.B. Salunkhe, V.M. Khot, M.R. Phadatare, N.D. Thorat, R.S. Joshi, H.M. Yadav, S.H. Pawar, Low temperature combustion synthesis and magnetostructural properties of Co-Mn nanoferrites. J. Magn. Magn. Mater. **352**(1), 91–98 (2014). https://doi.org/10.1016/j.jmmm.2013.09.020
16. M.K. Shobana, S. Sankar, Characterization of sol-gel-prepared nanoferrites. J. Magn. Magn. Mater. **321**(6), 599–601 (2009). https://doi.org/10.1016/j.jmmm.2008.09.040
17. R.H. Kodama, A.E. Berkowitz, E.J. McNiff Jr., S. Foner, Surface spin disorder in $NiFe_2O_4$ nanoparticles. Phys. Rev. Lett. **77**(2), 394–397 (1996)
18. B. Martínez, X. Obradors, L. Balcells, A. Rouanet, C. Monty, Low-temperature surface spin-glass transition in γ-Fe_2O_3 nanoparticles. Phys. Rev. Lett. **80**(1), 181–184 (1998)
19. Y. Köseoglu, H. Kavas, Size and surface effects on magnetic properties of Fe_3O_4 nanoparticles. J. Nanosci. Nanotechnol. **8**, 584 (2008)
20. S.D. Bhame, P.A. Joy, Tuning of the magnetostrictive properties of $CoFe_2O_4$ by Mn substitution for Co. J. Appl. Phys. **100**, 113911 (2006)
21. R.C. Kambale, P.A. Shaikh, N.S. Harale, V.A. Bilur, Y.D. Kolekar, C.H. Bhosale, K.Y. Rajpure, Structural and magnetic properties of Co1-xMnxFe2O4(0 {<=} x {<=} 0.4) spinel ferrites synthesized by combustion route. J Alloys Compd **490**(1–2), 568–571 (2010). https://doi.org/10.1016/j.jallcom.2009.10.082
22. M. Angelakeris, Magnetic nanoparticles: a multifunctional vehicle for modern theranostics. Biochim. Biophys. Acta - Gen. Subj. **1861**(6), 1642–1651 (2017)

23. A. Mumtaz, K. Maaz, B. Janjua, S.K. Hasanain, M.F. Bertino, Exchange bias and vertical shift in $CoFe_2O_4$ nanoparticles. J. Magn. Magn. Mater. **313**(2), 266–272 (2007). https://doi.org/10.1016/j.jmmm.2007.01.007
24. K.M. Batoo, D. Salah, G. Kumar, A. Kumar, M. Singh, M. Abd El-Sadek, F.A. Mir, A. Imran, D.A. Jameel, Hyperfine interaction and tuning of magnetic anisotropy of cu doped CoFe2O4 ferritenanoparticles. J. Magn. Magn. Mater. **411**, 91–97 (2016). https://doi.org/10.1016/j.jmmm.2016.03.058
25. M. Tachiki, Origin of the magnetic anisotropy energy of cobalt ferrite. Prog. Theor. Phys. **23**, 1055 (1960)
26. G. Dixit, J.P. Singh, R.C. Srivastava, H.M. Agrawal, Magnetic resonance study of Ce and Gd doped $NiFe_2O_4$. J. Magn. Magn. Mater. **324**(4), 479–483 (2014)
27. E. de Biasi, C.A. Ramos, R.D. Zysler, Size and anisotropy determination by ferromagnetic resonance in dispersed magnetic nanoparticle systems. J. Magn. Magn. Mater. **262**(2), 235–241 (2003)
28. J. Typek, K. Wardal, N. Guskos, D. Sibera, U. Narkiewicz, FMR and magnetization study of $ZnFe_2O_4$ nanoparticles in $_{0.40}Fe_2O_3/_{0.60}ZnO$ nanocomposite. IEEE J. Magn. Mater. **50**, 6101606 (2014)
29. D. Shi, B. Aktas, B. Pust, F. Mikailov, *Nanostructured Magnetic Materials, and Their Applications* (Springer- Verlag Inc., New York, 2003)
30. C. Vittoria, C.M. Williams, Ferrimagnetic resonance linewidth in single crystal MnZn-Ferrite. J. Magn. Magn. Mater. **54–57**(3), 1193–1194 (1986)
31. H.H. Hamdeh, J.C. Ho, S.A. Oliver, R.J. Willey, G. Oliveri, G. Busca, Magnetic properties of partially-inverted zinc ferrite aerogel powders. Phys. J. Appl. **81**, 1851 (1997)
32. G. Vázquez-Victorio, U. Acevedo-Salas, R. Valenzuela, in *Ferromagnetic Resonance - Theory and Applications*, ed. By O. Yalçin (IntechOpen, 2013), p. 169
33. L. Arda, M. Acikgoz, N. Doğan, D. Akcan, O. Cakiroglu, Synthesis, characterization and ESR studies of $Zn_{1-x}Co_xO$ nanoparticles. J. Supercond. Nov. Magn. **27**, 799 (2014)